Supporting Information for "Reassessing the Thermal Structure of Oceanic Lithosphere with Revised Global Inventories of Basement Depths and Heat Flow Measurements"

F.D. Richards[1,2], M.J. Hoggard[2], L.R. Cowton[3] & N.J. White[1]

Contents of this file

---

[1]Department of Earth Sciences, Bullard Laboratories, Madingley Rise, Madingley Road, Cambridge, CB3 0EZ, UK

[2]Department of Earth & Planetary Sciences, Harvard University, 20 Oxford Street, Cambridge, MA 02138, USA

[3]ASI Data Science, 54 Welbeck Street, London, W1G 9XS, UK

Additional Supporting Information (Files uploaded separately)

1. Captions for Dataset S1

Text S1

Density Parameterizations

Temperature-Dependent Parameterizations

For temperature dependent parameterizations, following the approach of *McKenzie et al.* [2005], density is given by

$$\rho = \rho_0 \exp\left(-\left[\alpha_0(T - T_0) + \frac{\alpha_1}{2}(T^2 - T_0^2)\right]\right). \tag{1}$$

α_0 and α_1 are calibrated constants derived from mineral physics experiments that describe the temperature dependence of thermal expansivity, $\rho_0 = 3.33$ Mg m^{-3} and $T_0 = 273$ K.

Temperature and Pressure-Dependent Parameterizations

For temperature and pressure-dependent parameterizations the approach of *Grose and Afonso* [2013] is adopted to determine density. First, isothermal volume change $(V_0/V)_T$ is calculated from pressure at each timestep using a Brent minimization algorithm and the third-order Birch-Murnaghan equation of state

$$P = \frac{3}{2}K_0\left[\left(\frac{V_0}{V}\right)_T^{\frac{7}{3}} - \left(\frac{V_0}{V}\right)_T^{\frac{5}{3}}\right]\left\{1 + \frac{3}{4}(K_T' - 4)\left[\left(\frac{V_0}{V}\right)_T^{\frac{2}{3}} - 1\right]\right\} \tag{2}$$

where $K_0 = 130$ GPa is the bulk modulus at $P = 0$ and $K_T' = 4.8$ is the pressure derivative of the isothermal bulk modulus. Having calculated isothermal volume change, isothermal density change as a function of pressure can then be calculated using

$$\rho(P) = \rho_0\left(\frac{V_0}{V}\right)_T. \tag{3}$$

Next the pressure dependence of thermal expansivity as a function of temperature is determined using

$$\frac{\alpha(P,T)}{\alpha(T)} = \left(\frac{V_0}{V}\right)_T \exp\left\{(\delta_T + 1)\left[\left(\frac{V_0}{V}\right)_T^{-1} - 1\right]\right\} \tag{4}$$

where $\delta_T = 6$ is the Grüneisen parameter. This expression then allows for density to be calculated as a function of temperature and pressure using

$$\rho(P,T) = \rho(P)\left(1 - \frac{\alpha(P,T)}{\alpha(T)}\int_{T_0}^{T}\alpha(T)dT\right). \tag{5}$$

Since the pressure effect in oceanic crust is minor, the same expressions and moduli are applied to the crustal layer.

Figures S1-S6

See pages 6–11.

Tables S1-S3

See pages 12–13.

Notation Table

See page 14.

Data Set S1

Adapted lithospheric age grid of *Müller et al.* [2016], augmented by including oceanic crust from the Black Sea, Caspian Sea, eastern Mediterranean Sea, New Caledonian and Aleutian basins. Gridding artefacts within the Gulf of California and along the Mohns Ridge are also corrected using age constraints taken from *Müller et al.* [2008].

References

Grose, C. J., and J. C. Afonso (2013), Comprehensive plate models for the thermal evolution of oceanic lithosphere, *Geochemistry, Geophys. Geosystems*, *14*(9), 3751–3778, doi:10.1002/ggge.20232.

Hofmeister, A. M. (2007), Pressure dependence of thermal transport properties, *Proc. Natl. Acad. Sci.*, *104*(22), 9192–9197, doi:10.1073/pnas.0610734104.

Korenaga, T., and J. Korenaga (2016), Evolution of young oceanic lithosphere and the meaning of seafloor subsidence rate, *J. Geophys. Res. Solid Earth*, *121*, 6315–6332, doi:10.1002/2016JB013395.

McKenzie, D., J. Jackson, and K. Priestley (2005), Thermal structure of oceanic and continental lithosphere, *Earth Planet. Sci. Lett.*, *233*(3-4), 337–349, doi: 10.1016/j.epsl.2005.02.005.

Müller, R. D., M. Sdrolias, C. Gaina, and W. R. Roest (2008), Age, spreading rates, and spreading asymmetry of the world's ocean crust, *Geochemistry, Geophys. Geosystems*, *9*(4), doi:10.1029/2007GC001743.

Müller, R. D., M. Seton, S. Zahirovic, S. E. Williams, K. J. Matthews, N. M. Wright, G. E. Shephard, K. T. Maloney, N. Barnett-moore, D. J. Bower, and J. Cannon (2016), Ocean basin evolution and global-scale reorganization events since Pangea breakup, *Annu. Rev. Earth Planet. Sci. Lett.*, April, 107–138, doi:10.1146/annurev-earth-060115-012211.

Parsons, B., and J. G. Sclater (1977), An analysis of the variation of ocean floor bathymetry and heat flow with age, *J. Geophys. Res.*, *82*(5), 803, doi: 10.1029/JB082i005p00803.

Stein, C. A., and S. Stein (1992), A model for the global variation in oceanic depth and heat flow with lithospheric age, *Nature*, *356*, 133–135, doi:10.1038/359123a0.

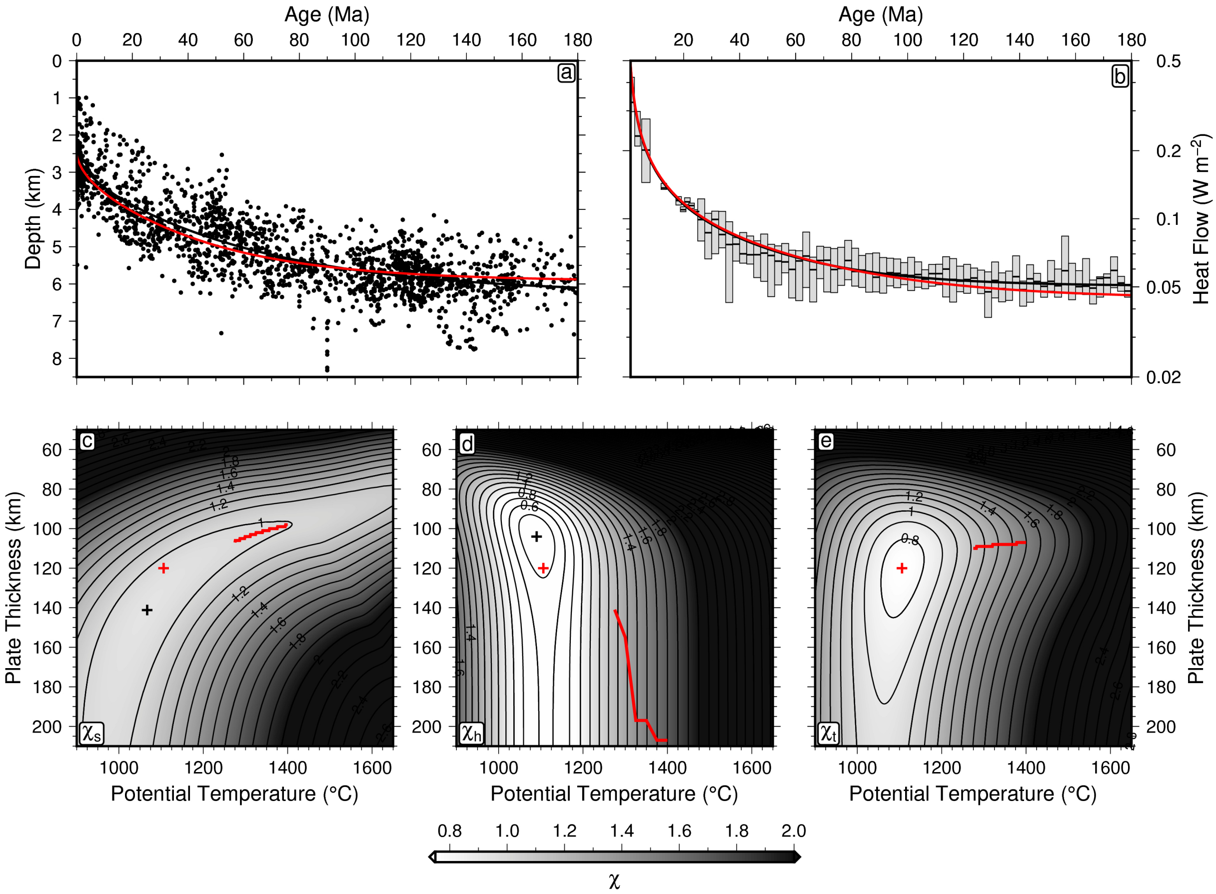

Figure S1: **Temperature-dependent plate model with updated conductivity parameterization of *Hofmeister* [2007] and no oceanic crust.** (a) Water-loaded depth to oceanic basement as function of plate age (Figure 2d); black line = optimal relationship obtained by only fitting age-depth observations; red line = optimal relationship from joint fit of age-depth and heat flow observations. (b) Surface heat flow as function of plate age (Figure 3c); gray boxes with horizontal bars = interquartile ranges of sediment-corrected heat flow measurements and median values; black line = optimal relationship obtained by only fitting heat flow observations; red line = optimal relationship from joint fit of age-depth and heat flow observations. (c) Misfit between observed and calculated age-depth observations, χ_s, as function of potential temperature and plate thickness, sliced at best fitting zero-age depth of 2.45 km; black cross = misfit minimum; red bar = optimal parameters when potential temperature is fixed at 1340 ± 60°C. (d) Same for misfit between observed and calculated heat flow, χ_h. (e) Same for joint misfit, χ_t, between observed and calculated age-depth and heat flow observations, sliced at best fitting zero-age depth of 2.55 km; red cross = global minimum used to generate red curves in panels (a) and (b).

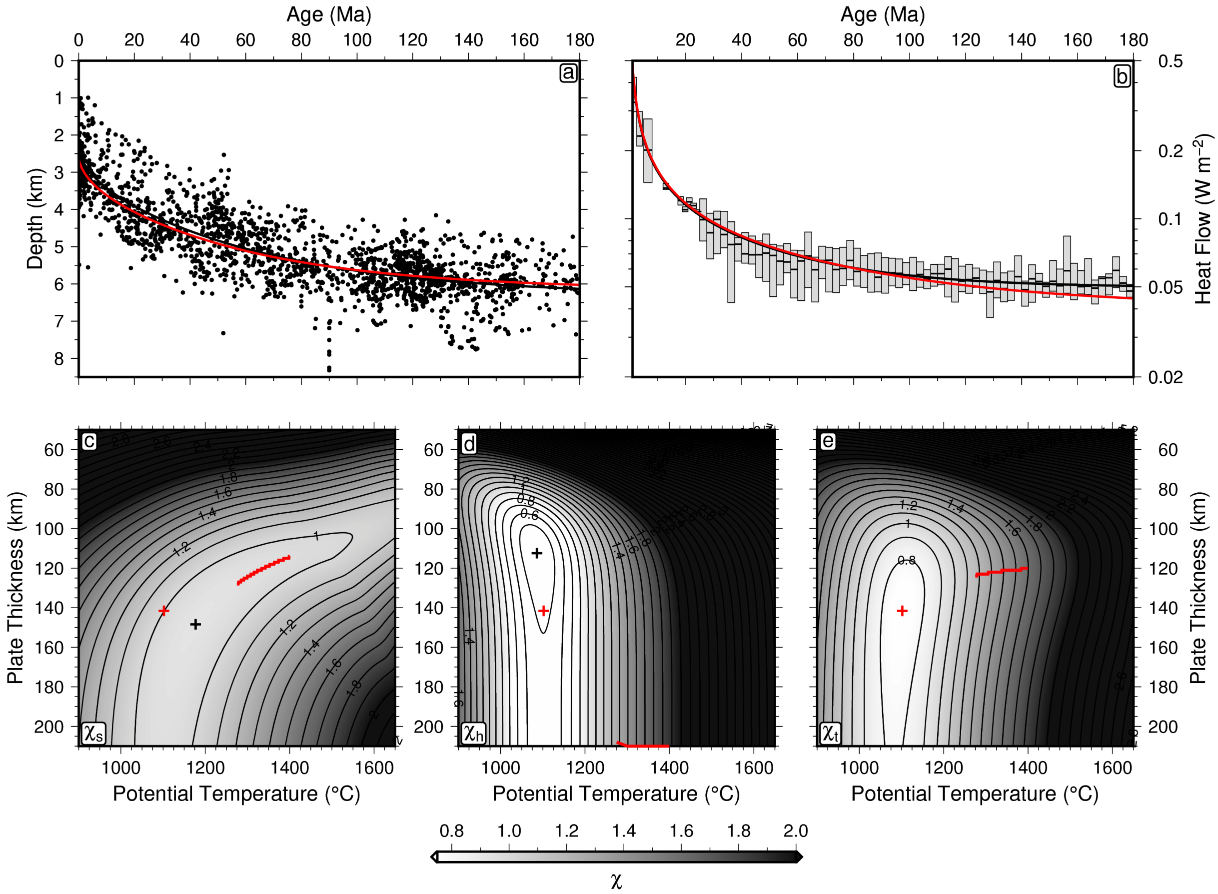

Figure S2: **Temperature-and pressure-dependent plate model with no oceanic crust.** (a) Water-loaded depth to oceanic basement as function of plate age (Figure 2d); black line = optimal relationship obtained by only fitting age-depth observations; red line = optimal relationship from joint fit of age-depth and heat flow observations. (b) Surface heat flow as function of plate age (Figure 3c); gray boxes with horizontal bars = interquartile ranges of sediment-corrected heat flow measurements and median values; black line = optimal relationship obtained by only fitting heat flow observations; red line = optimal relationship from joint fit of age-depth and heat flow observations. (c) Misfit between observed and calculated age-depth observations, χ_s, as function of potential temperature and plate thickness, sliced at best fitting zero-age depth of 2.45 km; black cross = misfit minimum; red bar = optimal parameters when potential temperature is fixed at $1340 \pm 60^{\circ}$C. (d) Same for misfit between observed and calculated heat flow, χ_h. (e) Same for joint misfit, χ_t, between observed and calculated age-depth and heat flow observations, sliced at best fitting zero-age depth of 2.65 km; red cross = global minimum used to generate red curves in panels (a) and (b).

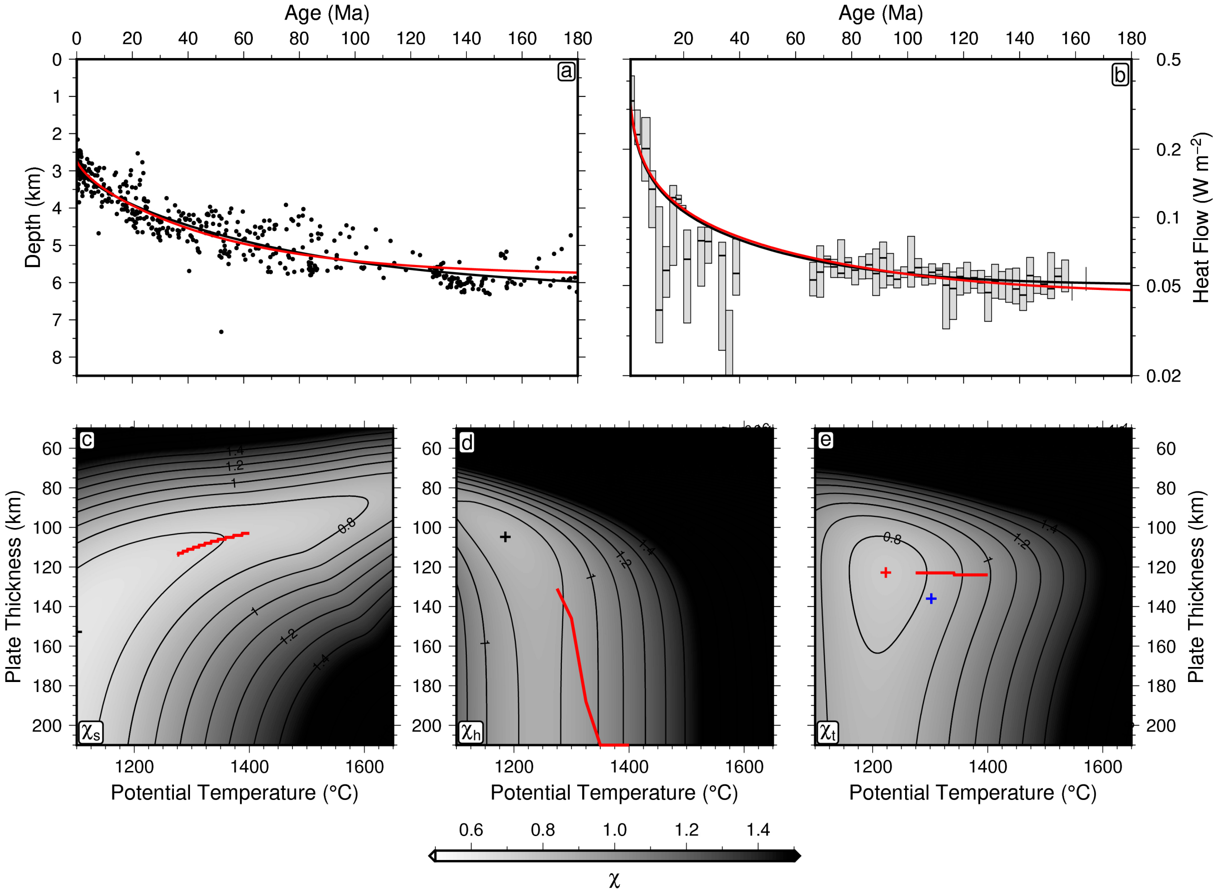

Figure S3: **Complete plate model with input data from Pacific Ocean only.** (a) Water-loaded depth to oceanic basement as function of plate age (Figure 2d); black line = optimal relationship obtained by only fitting age-depth observations; red line = optimal relationship from joint fit of age-depth and heat flow observations. (b) Surface heat flow as function of plate age (Figure 3c); gray boxes with horizontal bars = interquartile ranges of sediment-corrected heat flow measurements and median values; black line = optimal relationship obtained by only fitting heat flow observations; red line = optimal relationship from joint fit of age-depth and heat flow observations. (c) Misfit between observed and calculated age-depth observations, χ_s, as function of potential temperature and plate thickness, sliced at best fitting zero-age depth of 2.85 km; black cross = misfit minimum; red cross = joint misfit minimum used to generate red curves in panels (a) and (b); red bar = optimal parameters when potential temperature is fixed at 1340 ± 60°C. (d) Same for misfit between observed and calculated heat flow, χ_h. (e) Same for joint misfit, χ_t, between observed and calculated age-depth and heat flow observations, sliced at best fitting zero-age depth of 2.75 km; red cross = global minimum used to generate red curves in panels (a) and (b); blue cross = global minimum of global dataset.

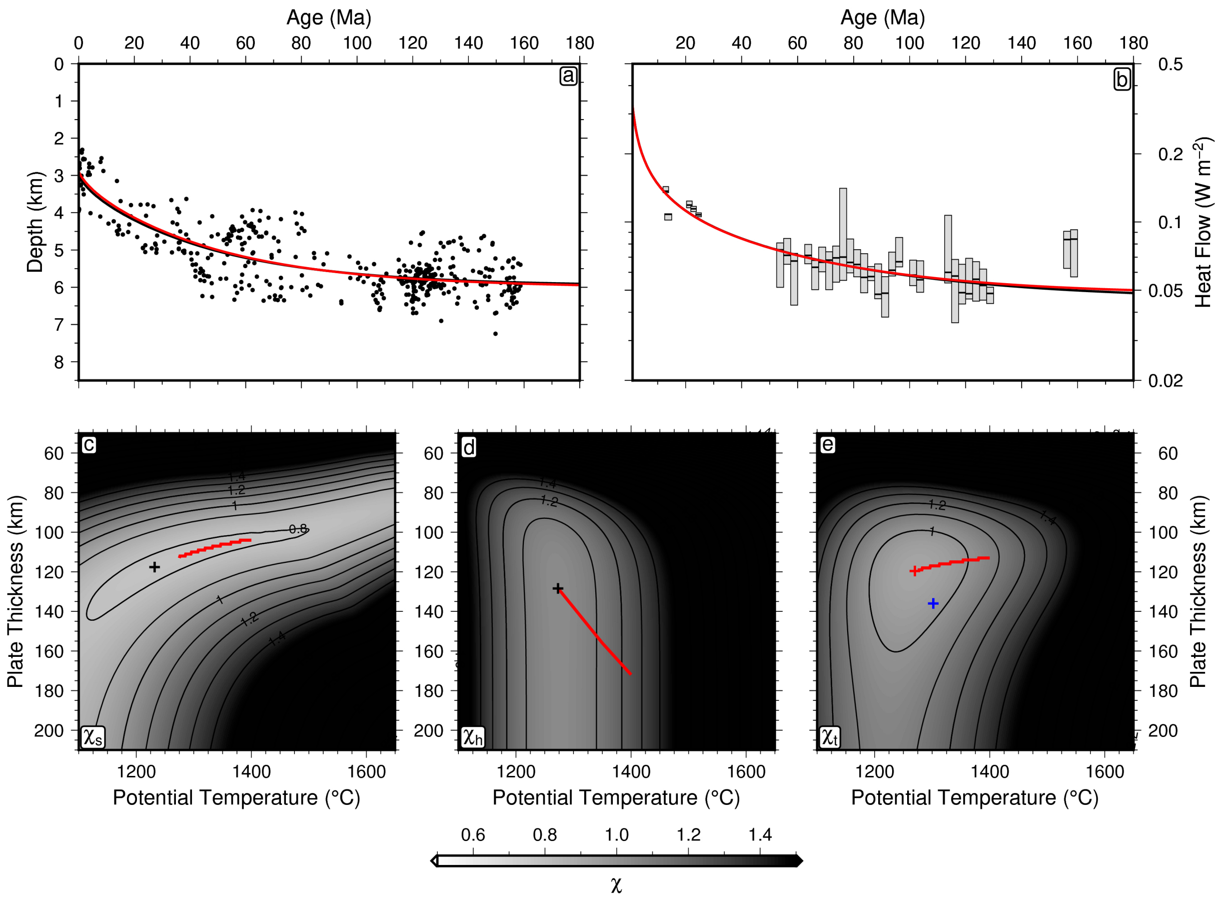

Figure S4: **Complete plate model with input data from Indian Ocean only.** (a) Water-loaded depth to oceanic basement as function of plate age (Figure 2d); black line = optimal relationship obtained by only fitting age-depth observations; red line = optimal relationship from joint fit of age-depth and heat flow observations. (b) Surface heat flow as function of plate age (Figure 3c); gray boxes with horizontal bars = interquartile ranges of sediment-corrected heat flow measurements and median values; black line = optimal relationship obtained by only fitting heat flow observations; red line = optimal relationship from joint fit of age-depth and heat flow observations. (c) Misfit between observed and calculated age-depth observations, χ_s, as function of potential temperature and plate thickness, sliced at best fitting zero-age depth of 3.00 km; black cross = misfit minimum; red cross = joint misfit minimum used to generate red curves in panels (a) and (b); red bar = optimal parameters when axial temperature is fixed at 1340 ± 60°C. (d) Same for misfit between observed and calculated heat flow, χ_h. (e) Same for joint misfit, χ_t, between observed and calculated age-depth and heat flow observations, sliced at best fitting zero-age depth of 2.90 km; red cross = global minimum used to generate red curves in panels (a) and (b); blue cross = global minimum of global dataset.

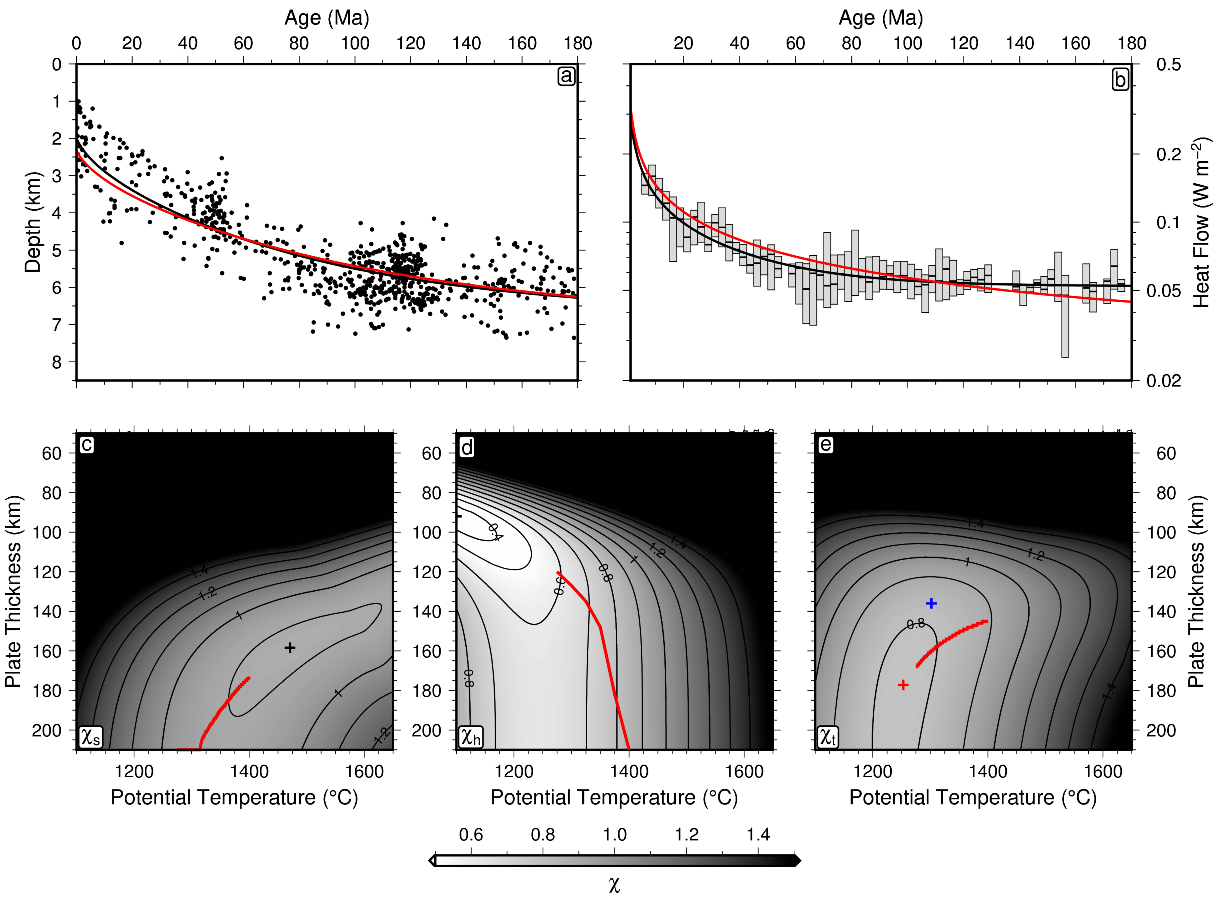

Figure S5: **Complete plate model with input data from Atlantic Ocean only.** (a) Water-loaded depth to oceanic basement as function of plate age (Figure 2d); black line = optimal relationship obtained by only fitting age-depth observations; red line = optimal relationship from joint fit of age-depth and heat flow observations. (b) Surface heat flow as function of plate age (Figure 3c); gray boxes with horizontal bars = interquartile ranges of sediment-corrected heat flow measurements and median values; black line = optimal relationship obtained by only fitting heat flow observations; red line = optimal relationship from joint fit of age-depth and heat flow observations. (c) Misfit between observed and calculated age-depth observations, χ_s, as function of potential temperature and plate thickness, sliced at best fitting zero-age depth of 2.00 km; black cross = misfit minimum; red cross = joint misfit minimum used to generate red curves in panels (a) and (b); red bar = optimal parameters when axial temperature is fixed at $1340 \pm 60^\circ$C. (d) Same for misfit between observed and calculated heat flow, χ_h. (e) Same for joint misfit, χ_t, between observed and calculated age-depth and heat flow observations, sliced at best fitting zero-age depth of 2.35 km; red cross = global minimum used to generate red curves in panels (a) and (b); blue cross = global minimum of global dataset.

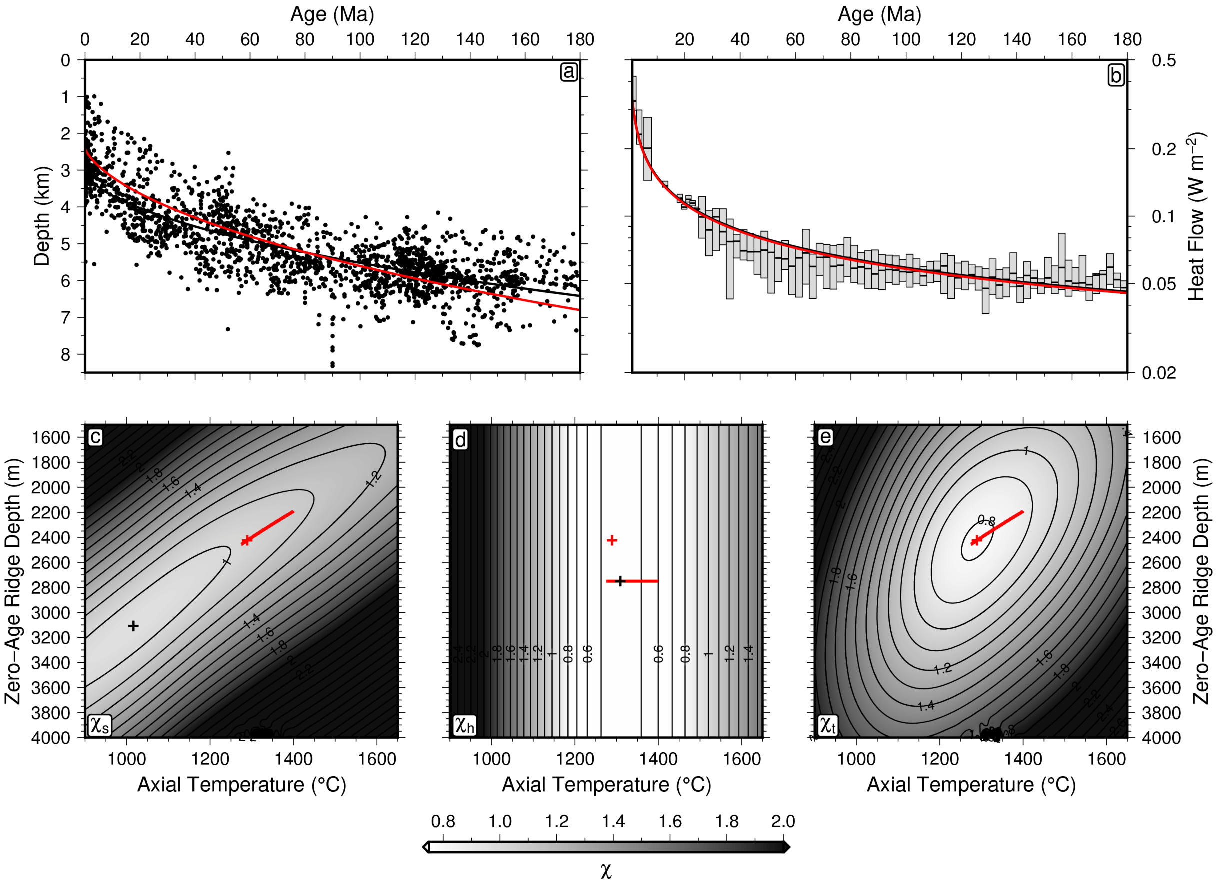

Figure S6: **Temperature-and pressure-dependent half-space cooling model including 7 km oceanic crustal layer.** (a) Water-loaded depth to oceanic basement as function of plate age (Figure 2d); black line = optimal relationship obtained by only fitting age-depth observations; red line = optimal relationship from joint fit of age-depth and heat flow observations. (b) Surface heat flow as function of plate age (Figure 3c); gray boxes with horizontal bars = interquartile ranges of sediment-corrected heat flow measurements and median values; black line = optimal relationship obtained by only fitting heat flow observations; red line = optimal relationship from joint fit of age-depth and heat flow observations. (c) Misfit between observed and calculated age-depth observations, χ_s, as function of axial temperature and zero-age ridge depth, sliced at best fitting zero-age depth of 3.15 km; black cross = misfit minimum; red bar = optimal parameters when axial temperature is fixed at 1340 ± 60°C. (d) Same for misfit between observed and calculated heat flow, χ_h. (e) Same for joint misfit, χ_t, between observed and calculated age-depth and heat flow observations, sliced at best fitting zero-age depth of 2.40 km; red cross = global minimum used to generate red curves in panels (a) and (b).

Table S1: **Comparison of thermal structure and seismic constraints.** T_S = seismogenic thickness-controlling isotherm for best-fit models; $[T_S]_{1333^\circ C}$ = seismogenic thickness-controlling isotherm for geochemically constrained models. z_L = average depth at $t \geq 100$ of T_L isotherm where $\phi = 0.843$ for best-fit models; $[z_L]_{1333^\circ C}$ = average depth at $t \geq 100$ Ma of T_L isotherm where $\phi = 0.843$ for geochemically constrained models; upper and lower bounds correspond to $\phi = 0.9$ and $\phi = 0.78$, respectively. Model names same as in Table 1.

Model	T_S (°C)	$[T_S]_{1333^\circ\mathrm{C}}$ (°C)	z_L (km)	$[z_L]_{1333^\circ\mathrm{C}}$ (km)
HSCk	728	653	132^{+20}_{-16}	131^{+20}_{-16}
Pk	760	685	96^{+7}_{-7}	82^{+5}_{-6}
MR*	630	606	90^{+4}_{-5}	88^{+4}_{-5}
KR	473	561	107^{+7}_{-8}	113^{+7}_{-8}
KRC	486	588	114^{+9}_{-10}	118^{+10}_{-10}
KRCCk	743	754	113^{+10}_{-10}	114^{+5}_{-11}
KRCC	694	706	109^{+10}_{-10}	110^{+10}_{-10}

Table S2: **Summary of previously published model results** PS77 = *Parsons and Sclater* [1977]; SS92 = *Stein and Stein* [1992]; MJP05 = *McKenzie et al.* [2005]; GA13 = *Grose and Afonso* [2013]; KK16 = *Korenaga and Korenaga* [2016]; RHCW18 = this study (KRCC model). * Fit is only calculated up to 100 Ma as model prediction is truncated at this age – others misfit calculations are carried out up to 170 Ma.

Model	χ_s	χ_{hf}	χ_t
PS77	0.947	1.035	0.992
SS92	1.007	0.446	0.779
MJP05	0.933	0.608	0.787
GA13	0.946	0.607	0.795
KK16*	1.419	0.520	1.069
RHCW18	0.931	0.442	0.729

Table S3: **Summary of model results** Details on model setup and best-fitting parameters for unconstrained mantle potential temperature and geochemically constrained temperature ($T_p = 1333°C$ equivalent to 7.1 km average crustal thickness). z_c = crustal thickness, MR* = parameters from *McKenzie et al.* [2005], GA13 = parameters from *Grose and Afonso* [2013] and KK16 = parameters from *Korenaga and Korenaga* [2016].

Model	$[T_P]_s$ (°C)	$[z_p]_s$ (km)	$[z_r]_s$ (m)	χ_s	$[T_P]_{hf}$ (°C)	$[z_p]_{hf}$ (km)	χ_{hf}
HSCk	1005	–	2816	0.951	1503	–	0.624
Pk	1307	129	2352	0.927	1474	92	0.416
MR*	1221	110	2548	0.927	1379	85	0.407
KR	1067	141	2432	0.927	1090	104	0.413
KRC	1147	151	2444	0.927	1086	112	0.410
KRCCk	1308	136	2684	0.928	1310	142	0.444
KRCC	1325	136	2604	0.927	1304	140	0.441

Table 4: **Notation table for parameters used in text.**

Notation	Parameter	Dimensions/Value
A	seafloor area	m^2
α	thermal expansivity	K^{-1}
C_p	specific heat capacity	J kg^{-1} K^{-1}
F	fractional disturbance of heat flow	dimensionless
G	gravitational constant	6.67$\times$ 10 $^{-11}$ m^3 kg^{-1} s^{-2}
Δg	gravity anomaly	m s^{-2}
H	heat flow	W m^{-2}
k	thermal conductivity	W m^{-1} K^{-1}
k_{lat}	lattice thermal conductivity	W m^{-1} K^{-1}
k_{rad}	radiative thermal conductivity	W m^{-1} K^{-1}
κ	thermal diffusivity	m^2 s^{-1}
l	spherical harmonic degree	dimensionless
λ	longitude	$^\circ$
Q	cumulative oceanic heat flow	TW
m	spherical harmonic order	dimensionless
P	pressure	Pa
ϕ	critical isotherm coefficient	dimensionless
R	Earth radius	6371 km
ρ	density	kg m^{-3}
ρ_b	density at compensation depth	kg m^{-3}
ρ_m	mantle density	kg m^{-3}
ρ_w	water density	kg m^{-3}
S	sedimentation rate	m s^{-1}
t	time	s
Δt	finite difference timestep	s
ΔU	gravitational potential anomaly	m^2 s^{-2}
T	temperature	$^\circ$C
T_0	surface temperature	$^\circ$C
T_L	critical isotherm defining lithospheric thickness	$^\circ$C
T_p	mantle potential temperature	$^\circ$C
θ	co-latitude	$^\circ$
X	composition	dimensionless
χ_{hf}	heat flow misfit	dimensionless
χ_s	subsidence misfit	dimensionless
χ_t	joint misfit	dimensionless
z_c	crustal thickness	km
z_p	plate thickness	km
z_r	zero-age ridge depth	m
Δz	finite difference depth spacing	m
w	water-loaded oceanic basement depth	m